

Crystal Dynamics of Potassium. II. The Anharmonic Effects

W. J. L. BUYERS AND R. A. COWLEY

Chalk River Nuclear Laboratories, Atomic Energy of Canada Limited, Chalk River, Ontario, Canada

(Received 12 November 1968)

The frequencies and the lifetimes of the normal modes of vibration of potassium have been measured at four different temperatures with neutron inelastic scattering techniques. The changes in the results with temperature were found to be in reasonable agreement with calculations of the effect of anharmonicity on the normal modes. Up to nine-tenths of the melting temperature, the temperature dependence of the frequencies and of the thermal expansion coefficient was found to be in agreement with calculations based on the neutral-pseudoatom model of a crystal. The agreement between experiment and calculation for the lifetime of the normal modes was less satisfactory. The discrepancy may in part be due to the difficulty in extracting the instrumental resolution function. The neutral-pseudoatom potential used in these calculations was derived from the frequencies of the normal modes of vibration at low temperature, as described previously. It is shown that the neutral-pseudoatom model for the anharmonic effects neglects interactions between three or more ions which are present in more exact theories. The agreement obtained between experiment and theory therefore suggests that the many-body forces are smaller than the two-body forces. We also describe the effect of anharmonicity on the strength of Kohn anomalies in metals; one contribution to their strength has the same temperature dependence as the Debye-Waller factor.

1. INTRODUCTION

IN this paper we describe experimental measurements and theoretical calculations of the effects of anharmonicity in potassium metal. The experimental measurements were made by coherent one-phonon scattering of slow neutrons from a single crystal of potassium. Earlier measurements¹ of the phonons were made at 9°K, and in this work we studied the changes in several of these phonons when the temperature of the crystal was raised to 92, 215, and 299°K.

The theory of simple metals has received considerable impetus from the introduction of the concept of a pseudopotential² for the electron-phonon interaction. By now a large number of authors³⁻⁶ have used the pseudopotential technique to calculate the phonon dispersion relations of simple metals, while others have constructed these potentials from the measured dispersion relations.¹ When an ion moves, the conduction electrons move so as to screen the long-range electrostatic fields. The ions and their associated screening clouds of electrons, known as neutral pseudoatoms, may be shown to interact with one another through a relatively short-range potential,⁷ as is confirmed by the experimental measurements.

A more severe test of this theory is the extent to which it may be used to calculate anharmonic effects. In this paper, extensive measurements of phonon frequencies and lifetimes at several temperatures are compared with calculations of the effects on the basis of the pseudopotential theory.

In Sec. 2 we describe inelastic neutron scattering measurements of the phonons in potassium and obtain the change in the frequency and lifetime with increasing temperature. In Sec. 3 we describe the harmonic and anharmonic pseudopotential theory within the neutral-pseudoatom approximation. This is then used to calculate the thermal expansion, which in Sec. 4 is shown to be in good agreement with experiment. The phonon self-energy is calculated in Sec. 5, and fairly good agreement is found when experiment and theory are compared in Sec. 6. An analysis of the pseudopotential method is given in Sec. 7, where the detailed structure of the ion-electron-ion interaction is shown to lead to more complex anharmonic interactions than those we have considered. It is shown that the neutral-pseudoatom approximation is equivalent to including only a particular class of interaction. In addition, some interesting effects of temperature on Kohn anomalies are predicted. Our conclusions are summarized in Sec. 8.

2. NEUTRON SCATTERING MEASUREMENTS

A. Experiment

Measurements were made of the inelastic neutron scattering from a single crystal of potassium with a triple-axis spectrometer at the NRU reactor, Chalk River. The crystal was aligned so that scattering took place

TABLE I. Instrumental resolution.

	Incident beam	Scattered beam
Collimation: Horizontal	0.70°	0.65°
Vertical	1°	4°
Monochromating crystal:	Al, mosaic spread 0.48°	
Analyzing crystal:	Al, mosaic spread 0.63°	
A: (111) Analyzer planes at 67°	For modes Δ_1 , Σ_3 , and	
(111) Monochromator planes	Δ_5 with $\zeta \leq 0.6$	
B: (111) Analyzer planes at 65°	For modes Σ_1 , Δ_3 , and	
(200) Monochromator planes	Δ_5 with $\zeta > 0.6$	

¹ R. A. Cowley, A. D. B. Woods, and G. Dolling, *Phys. Rev.* **150**, 487 (1966).

² L. J. Sham and J. M. Ziman, *Solid State Phys.* **15**, 221 (1963).

³ L. J. Sham, *Proc. Roy. Soc. (London)* **A283**, 33 (1965).

⁴ T. Schneider and E. Stoll, *Physik Kondensierten Materie* **5**, 331 (1966).

⁵ N. W. Ashcroft, *J. Phys.* **C1**, 232 (1968).

⁶ W. A. Harrison, *Phys. Rev.* **129**, 2522 (1963).

⁷ J. M. Ziman, *Advan. Phys.* **13**, 89 (1964).

TABLE II. Measured widths and shifts in K, in units of 10^{12} Hz. The table shows the position in reciprocal space, $(2\pi/a)(Q_x, Q_y, Q_z)$, where the phonon was observed; its frequency ν ; and its full width at half-height, W , at the lowest temperature (9°K). The width is taken as the resolution width of the spectrometer for each phonon. The changes in frequency $\delta\Delta$ and in the natural half-width $\delta\Gamma$, that have been derived from measurements at higher temperature T , are shown in the final columns.

Q_x	Q_y	Q_z	ν	W	T	Shift $\delta\Delta$	Half-width $\delta\Gamma$
2.0	2.0	0.2	0.68 \pm 0.025	0.13 \pm 0.03	299	-0.16 \pm 0.03	0.03 \pm 0.03
Δ_5					215	-0.09 \pm 0.03	0.00 \pm 0.03
2.0	2.0	0.3	0.99 \pm 0.02	0.10 \pm 0.03	299	-0.19 \pm 0.03	0.04 \pm 0.04
Δ_5					215	-0.12 \pm 0.03	0.04 \pm 0.04
2.0	2.0	0.4	1.28 \pm 0.025	0.09 \pm 0.03	299	-0.20 \pm 0.04	0.11 \pm 0.04
Δ_5					215	-0.12 \pm 0.03	0.07 \pm 0.03
2.0	2.0	0.5	1.56 \pm 0.02	0.13 \pm 0.03	299	-0.23 \pm 0.04	0.06 \pm 0.05
Δ_5					215	-0.13 \pm 0.03	0.06 \pm 0.04
2.0	2.0	0.6	1.79 \pm 0.025	0.13 \pm 0.03	299	-0.26 \pm 0.05	0.08 \pm 0.05
Δ_5					215	-0.15 \pm 0.04	0.09 \pm 0.04
					92	-0.04 \pm 0.03	0.02 \pm 0.04
2.0	2.0	0.7	1.98 \pm 0.02	0.14 \pm 0.03	299	-0.26 \pm 0.04	0.08 \pm 0.05
Δ_5					215	-0.15 \pm 0.04	0.06 \pm 0.04
					92	-0.06 \pm 0.04	0.04 \pm 0.04
2.0	2.0	0.75	2.07 \pm 0.03	0.14 \pm 0.03	299	-0.23 \pm 0.04	0.10 \pm 0.04
Δ_5					215	-0.16 \pm 0.04	0.06 \pm 0.04
2.0	2.0	0.8	2.11 \pm 0.025	0.22 \pm 0.03	299	-0.24 \pm 0.04	0.05 \pm 0.06
Δ_5					215	-0.14 \pm 0.05	0.08 \pm 0.05
					92	-0.03 \pm 0.05	0.00 \pm 0.04
2.0	2.0	0.85	2.19 \pm 0.03	0.22 \pm 0.04	299	-0.26 \pm 0.08	0.10 \pm 0.09
Δ_5					215	-0.19 \pm 0.05	0.04 \pm 0.05
2.0	2.0	0.9	2.20 \pm 0.03	0.21 \pm 0.03	299	-0.24 \pm 0.04	0.06 \pm 0.05
Δ_5					215	-0.19 \pm 0.04	0.05 \pm 0.05
					92	-0.07 \pm 0.05	0.04 \pm 0.04
2.0	2.0	1.0	2.225 \pm 0.02	0.16 \pm 0.03	299	-0.16 \pm 0.07	0.15 \pm 0.08
H_{15}					215	-0.17 \pm 0.05	0.21 \pm 0.05
					92	-0.06 \pm 0.04	0.03 \pm 0.04
1.0	1.0	3.0	2.225 \pm 0.03	0.16 \pm 0.04	215	-0.19 \pm 0.04	0.11 \pm 0.04
H_{15}					92	-0.10 \pm 0.05	0.10 \pm 0.05
1.2	1.2	2.8	2.16 \pm 0.03	0.30 \pm 0.05	215	-0.16 \pm 0.04	0.00 \pm 0.05
F_3					92	-0.06 \pm 0.04	0.04 \pm 0.06
1.3	1.3	2.7	2.11 \pm 0.04	0.36 \pm 0.05	215	0.12 \pm 0.06	0.05 \pm 0.06
F_3					92	-0.04 \pm 0.09	0.05 \pm 0.07
1.4	1.4	2.6	1.89 \pm 0.04	0.39 \pm 0.06	215	-0.02 \pm 0.06	0.00 \pm 0.09
F_3					92	0.00 \pm 0.08	0.08 \pm 0.10
1.5	1.5	2.5	1.75 \pm 0.04	0.27 \pm 0.05	215	0.02 \pm 0.06	0.09 \pm 0.07
P_4					92	0.00 \pm 0.06	0.09 \pm 0.07
1.5	1.5	1.5	1.79 \pm 0.05	0.16 \pm 0.05	299	-0.23 \pm 0.06	0.21 \pm 0.05
P_4					215	-0.12 \pm 0.06	0.11 \pm 0.06
					92	-0.06 \pm 0.05	0.00 \pm 0.05
1.4	1.4	1.4	1.255 \pm 0.03	0.18 \pm 0.04	299	-0.24 \pm 0.04	0.11 \pm 0.04
F_1					215	-0.13 \pm 0.04	0.13 \pm 0.05
					92	-0.04 \pm 0.04	0.04 \pm 0.05
1.35	1.35	1.35	1.05 \pm 0.03	0.19 \pm 0.04	299	-0.18 \pm 0.04	0.06 \pm 0.06
F_1					215	-0.09 \pm 0.04	0.04 \pm 0.05
					92	-0.05 \pm 0.03	0.03 \pm 0.04
1.7	1.7	1.7	-1.02 \pm 0.03	0.16 \pm 0.03	299	-0.10 \pm 0.04	0.11 \pm 0.04
F_1					215	-0.08 \pm 0.04	0.10 \pm 0.04
					92	-0.03 \pm 0.03	0.04 \pm 0.03
1.75	1.75	0.75	1.20 \pm 0.03	0.12 \pm 0.03	299	-0.17 \pm 0.04	0.14 \pm 0.04
F_1					215	-0.10 \pm 0.04	0.06 \pm 0.03
1.8	1.8	1.8	1.475 \pm 0.02	0.15 \pm 0.03	299	-0.20 \pm 0.04	0.10 \pm 0.04
F_1					215	-0.12 \pm 0.03	0.08 \pm 0.04
					92	-0.05 \pm 0.03	0.02 \pm 0.03
1.6	1.6	1.6	2.12 \pm 0.04	0.25 \pm 0.04	299	-0.17 \pm 0.08	0.05 \pm 0.07
Λ_1					215	-0.10 \pm 0.05	0.04 \pm 0.07
					92	-0.04 \pm 0.05	0.00 \pm 0.05
2.3	2.3	0.3	2.13 \pm 0.04	0.19 \pm 0.04	299	-0.27 \pm 0.09	0.03 \pm 0.09
Λ_1					215	-0.12 \pm 0.06	0.13 \pm 0.06
					92	-0.09 \pm 0.05	0.06 \pm 0.05
2.2	2.2	0.2	1.68 \pm 0.03	0.18 \pm 0.04	299	-0.21 \pm 0.04	0.08 \pm 0.05
Λ_1					215	-0.13 \pm 0.04	0.07 \pm 0.05
					92	-0.06 \pm 0.04	0.00 \pm 0.04
2.1	2.1	0.1	0.94 \pm 0.02	0.12 \pm 0.02	299	-0.19 \pm 0.03	0.06 \pm 0.04
Λ_1					215	-0.06 \pm 0.03	0.04 \pm 0.03
					92	-0.05 \pm 0.03	0.02 \pm 0.03
1.4	1.4	1.0	0.81 \pm 0.03	0.11 \pm 0.03	299	-0.09 \pm 0.04	0.15 \pm 0.03
G_1					215	-0.04 \pm 0.04	0.05 \pm 0.04
					92	-0.01 \pm 0.03	0.02 \pm 0.02
1.5	1.5	1.0	0.53 \pm 0.02	0.16 \pm 0.03	299	-0.01 \pm 0.03	0.05 \pm 0.05
N_4'					215	0.01 \pm 0.03	0.05 \pm 0.05
					92	-0.01 \pm 0.02	0.02 \pm 0.03

TABLE II. (continued).

Q_x	Q_y	Q_z	ν	W	T	Shift $\delta\Delta$	Half-width $\delta\Gamma$
2.25 Σ_1	2.25	0.0	1.695±0.05	0.25±0.05	299	-0.19±0.06	0.00±0.05
					215	-0.11±0.06	0.00±0.06
					92	-0.05±0.06	0.00±0.06
2.3 Σ_1	2.3	0.0	1.93 ±0.05	0.24±0.09	299	-0.19±0.06	0.08±0.08
					215	-0.08±0.06	0.05±0.09
					92	-0.06±0.06	0.00±0.05
2.4 Σ_1	2.4	0.0	2.27 ±0.04	0.30±0.06	299	-0.18±0.06	0.11±0.09
					215	-0.10±0.06	0.08±0.09
					92	-0.05±0.06	0.04±0.06
2.5 N_1'	2.5	0.0	2.385±0.05	0.31±0.06	92	-0.06±0.07	0.00±0.06
0.85 Σ_3	0.85	2.0	0.66 ±0.01	0.08±0.02	299	-0.05±0.02	0.06±0.02
					215	-0.04±0.01	0.02±0.02
					92	0.01±0.01	
0.75 Σ_3	0.75	2.0	1.10 ±0.02	0.12±0.02	299	-0.06±0.03	0.06±0.03
					215	-0.11±0.03	0.04±0.03
					92	-0.02±0.02	0.02±0.02
0.65 Σ_3	0.65	2.0	1.355±0.02	0.10±0.02	299	-0.17±0.05	0.13±0.04
					215	-0.12±0.03	0.08±0.02
					92	-0.04±0.03	0.05±0.02

in the $(\bar{1}10)$ plane of the crystal. All measurements were of neutron-energy-loss processes with variable incident energy and fixed scattered energy under conditions set out in Table I. The constant- \mathbf{Q} technique⁸ was used throughout. Results have been obtained at four temperatures, 9, 92, 215, and 299°K, for about 30 phonons having the symmetries Δ_5 , Σ_1 , Σ_3 , $\Lambda_1(F_1)$, $\Lambda_3(F_3)$, and G_1 . The results at 9°K were already available from the work described in part I of this series.¹

Before presenting the results we shall describe our method employed for obtaining reliable phonon self-energies (i.e., widths and frequencies of the neutron groups to good accuracy in this experiment) from the total observed neutron intensity $S(\mathbf{Q},\Omega)$.

B. Contributions to Observed Scattering

The total scattering cross section contains coherent and incoherent scattering from both one- and multiphonon processes. Typical results at one wave vector are shown in Fig. 1. The one-phonon coherent cross section [see Eq. (10)] is strongly peaked in frequency, whereas the other contributions are expected to vary comparatively slowly with frequency. A flat background was therefore drawn under the one-phonon peak so that the width and center of gravity of the latter may be estimated. This simple procedure becomes less reliable at higher temperatures. At room temperature the multiphonon scattering was often greater than the one-phonon scattering, as shown in Fig. 1, where the multiphonon intensity in the experiment at 299°K was about twice the one-phonon peak intensity. It is clear nevertheless from Fig. 1 that despite the large multiphonon scattering it is still possible to estimate a one-phonon width and frequency from the results. The integrated

intensities shown in Fig. 1, which depend on the population factor and the Debye-Waller factor, are consistent with a Debye temperature of 70°K.

C. Instrumental Resolution

The finite instrumental resolution influences the measured position and width of the neutron groups. The observed intensity is the convolution of the instrumental resolution function as a function of \mathbf{Q} and Ω with the response of the crystal. Thus the observed width of a one-phonon group depends on where it is observed in (\mathbf{Q},Ω) space. Each neutron group was therefore measured as a function of temperature at the same position in reciprocal space and at the same resolution. The widths and shifts with temperature obtained by comparing the groups at high temperature with the groups at the lowest temperature should therefore be largely independent of instrumental resolution. Resolution elements are given in Table I.

D. Method of Extracting Phonon Widths and Shifts

For each momentum transfer, the frequency $\nu(T)$ and the full width at half-height, $W(T)$, were obtained at four temperatures. The derived widths and changes in the frequencies of the phonons are shown in Table II.

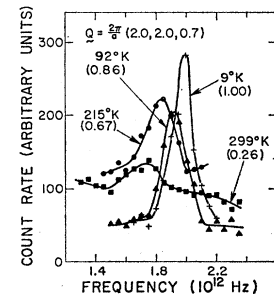


FIG. 1. Behavior of a neutron group in K as the temperature is raised. The figures in brackets below the temperatures are the peak intensities relative to that at 90°K and show how the Debye-Waller factor dominates the cross section for this phonon.

⁸ B. N. Brockhouse, in *Inelastic Scattering of Slow Neutrons from Solids and Liquids* (International Atomic Energy Agency, Vienna, 1961), p. 113.

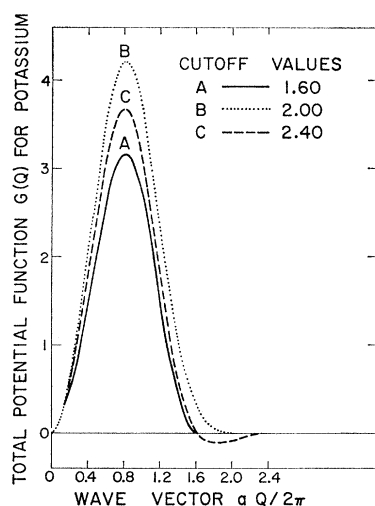


FIG. 2. The total potential in K derived from the low-temperature phonon frequencies and the elastic constants. The dimensionless function $G(Q) = (Q^2/e^2)\phi(Q)$ is plotted for various cutoff points in the fitting procedure to demonstrate that the potential derived is essentially independent of the range.

The change in the phonon frequency from its value at the lowest temperature (9°K) is given by the quantity

$$\delta\Delta(T) = \nu(T) - \nu(9),$$

which may then be compared with the $\delta\Delta(T)$ predicted by theory. The error in $\delta\Delta(T)$ is computed from the independent random errors in the two frequencies.

The change in the half-width, $\delta\Gamma(T)$, is not so easy to obtain because it is convoluted with the instrumental resolution. For each momentum transfer we assume that there is some instrumental function, Gaussian as a function of frequency, and independent of temperature, that will reproduce the observed one-phonon-neutron group when convoluted with the crystal response. As the form of the one-phonon cross section is approximately a Lorentzian (Sec. 5), the observed neutron group is a convolution of a Gaussian and a Lorentzian. The width of the instrumental resolution function is just that of the neutron group at 9°K , since the natural width at that temperature is negligible. For other temperatures, the natural width of the phonon was obtained by finding the width of the Lorentzian curve that must be convoluted with the resolution function so as to give the observed width. The error in the natural width was obtained by changing the observed width by its error and repeating the deconvolution procedure. In the few cases where the natural width at 9°K is not negligible, the phonon width obtained by the deconvoluting procedure is an approximate measure of $\delta\Gamma$, the change in width as the temperature is raised, and it is this quantity that is chosen for comparison of the theory and experiment. Little difference in the estimated phonon width is made by assuming that it has a Gaussian line shape provided its width is significantly larger than the resolution width. When the widths are com-

parable, however, the forms taken for the line shape and for the resolution function make a considerable difference to the results.

E. Results

With the above method, the phonon widths and shifts shown in Table II have been obtained. Both quantities increase in magnitude markedly with increasing temperature and are wave-vector-dependent. Typical phonon frequencies are reduced by 16% at room temperature and have lifetimes of the order of 10 periods of vibration. In a case where, because of the errors present, the width observed was less than that at 9°K , the tabulated change in width $\delta\Gamma$ is always set to zero.

From Table II it may be seen that the changes in the frequencies with temperature have at best been measured to an accuracy of 20%. The accuracy in the half-widths is considerably worse. These errors arise largely from the errors introduced in the deconvoluting process, for the errors in the widths of the neutron groups are comparable to the errors of their frequencies. Although many of the widths are not significant by themselves, it is nevertheless the case that the over-all trend of any group of results is likely significant.

3. PSEUDOATOM THEORY

A. Harmonic Approximation

In simple metals, such as potassium, the interionic forces arise from the direct Coulomb forces and from the ion-electron-ion forces and may be combined to give an effective short-range potential $\phi(R)$, between neutral pseudoatoms⁷ distance R apart. It is convenient to evaluate the expression for the frequencies of the normal modes of vibration in terms of the Fourier transform of the potential $\phi(Q)$:

$$\phi(R) = \int \phi(Q) e^{i\mathbf{Q}\cdot\mathbf{R}} \frac{d^3Q}{(2\pi)^3}. \quad (1)$$

The phonon frequency $\omega(\mathbf{q}j)$ of a normal mode of wave vector \mathbf{q} and eigenvector $u_\alpha(\mathbf{q}j)$ is then given by¹

$$\omega^2(\mathbf{q}j) = \frac{1}{Mv} \sum_{\alpha\beta} \sum_{\boldsymbol{\tau}} [(\mathbf{q}+\boldsymbol{\tau})_\alpha(\mathbf{q}+\boldsymbol{\tau})_\beta \phi(|\mathbf{q}+\boldsymbol{\tau}|) - \tau_\alpha\tau_\beta \phi(|\boldsymbol{\tau}|)] u_\alpha(\mathbf{q}j) u_\beta(-\mathbf{q}j), \quad (2)$$

where M is the mass of the atom, v is the volume of the unit cell, and $\boldsymbol{\tau}$ is a reciprocal lattice vector.

The function $\phi(Q)$ for sodium and potassium were obtained earlier¹ from the experimental measurements of the phonon frequencies at 9°K . These results were improved for the present calculations by fitting the functions not only to the observed phonon frequencies but also to the measured elastic constants. Figure 2 shows that, in contrast to the results obtained earlier, these did not show any appreciable dependence on the

cutoff chosen for the function $\phi(Q)$, and are correspondingly considerably more satisfactory. Some of the calculations reported below were made using functions with different cutoffs, but the results were not much altered by the cutoff as discussed later in Sec. 4. Most of the calculations were therefore performed with a cutoff of 1.6.

B. Anharmonic Potential

The calculation of the temperature dependence of the properties of a crystal is performed by expanding the potential in a power series of the phonon coordinates,⁹

$$V_{\text{anh}} = \sum_{1,2,3} V(\mathbf{q}_1 j_1, \mathbf{q}_2 j_2, \mathbf{q}_3 j_3) A(\mathbf{q}_1 j_1) A(\mathbf{q}_2 j_2) A(\mathbf{q}_3 j_3) \\ + \sum_{1,2,3,4} V(\mathbf{q}_1 j_1, \mathbf{q}_2 j_2, \mathbf{q}_3 j_3, \mathbf{q}_4 j_4) \\ \times A(\mathbf{q}_1 j_1) A(\mathbf{q}_2 j_2) A(\mathbf{q}_3 j_3) A(\mathbf{q}_4 j_4) + \dots, \quad (3)$$

where $A(\mathbf{q}j)$ is the sum of phonon creation and destruction operators. The coefficients in this expansion are given in terms of the real space derivatives of the interatomic potential by Born and Huang.¹⁰ In terms of $\phi(Q)$, they are

$$V(\mathbf{q}_1 j_1, \mathbf{q}_2 j_2, \mathbf{q}_3 j_3) \\ = \frac{\Delta(\mathbf{q}_1 + \mathbf{q}_2 + \mathbf{q}_3)}{N^{1/2} M^{3/2} 3!} \left(\frac{\hbar^3}{8\omega(\mathbf{q}_1 j_1)\omega(\mathbf{q}_2 j_2)\omega(\mathbf{q}_3 j_3)} \right)^{1/2} \\ \times \sum_{\alpha\beta\gamma} \{H_3(\mathbf{q}_1) + H_3(\mathbf{q}_2) + H_3(\mathbf{q}_3)\}_{\alpha\beta\gamma} \\ \times u_\alpha(\mathbf{q}_1 j_1) u_\beta(\mathbf{q}_2 j_2) u_\gamma(\mathbf{q}_3 j_3), \quad (4)$$

where

$$\{H_3(\mathbf{q})\}_{\alpha\beta\gamma} = -\frac{i^3}{v} \sum_{\tau} (\mathbf{q} + \boldsymbol{\tau})_\alpha (\mathbf{q} + \boldsymbol{\tau})_\beta (\mathbf{q} + \boldsymbol{\tau})_\gamma \phi(|\mathbf{q} + \boldsymbol{\tau}|)$$

and

$$V(\mathbf{q}_1 j_1, \mathbf{q}_2 j_2, \mathbf{q}_3 j_3, \mathbf{q}_4 j_4) \\ = \frac{\Delta(\mathbf{q}_1 + \mathbf{q}_2 + \mathbf{q}_3 + \mathbf{q}_4)}{NM^2 4!} \left(\frac{\hbar^4}{16\omega(\mathbf{q}_1 j_1)\omega(\mathbf{q}_2 j_2)\omega(\mathbf{q}_3 j_3)\omega(\mathbf{q}_4 j_4)} \right)^{1/2} \\ \times \sum_{\alpha\beta\gamma\delta} \{H_4(\mathbf{q}_1) + H_4(\mathbf{q}_2) + H_4(\mathbf{q}_3) + H_4(\mathbf{q}_4) \\ - H_4(\mathbf{q}_1 + \mathbf{q}_2) - H_4(\mathbf{q}_1 + \mathbf{q}_3) - H_4(\mathbf{q}_1 + \mathbf{q}_4) - H_4(0)\}_{\alpha\beta\gamma\delta} \\ \times u_\alpha(\mathbf{q}_1 j_1) u_\beta(\mathbf{q}_2 j_2) u_\gamma(\mathbf{q}_3 j_3) u_\delta(\mathbf{q}_4 j_4),$$

where

$$\{H_4(\mathbf{q})\}_{\alpha\beta\gamma\delta} = -\frac{i^4}{v} \sum_{\tau} (\mathbf{q} + \boldsymbol{\tau})_\alpha (\mathbf{q} + \boldsymbol{\tau})_\beta \\ \times (\mathbf{q} + \boldsymbol{\tau})_\gamma (\mathbf{q} + \boldsymbol{\tau})_\delta \phi(|\mathbf{q} + \boldsymbol{\tau}|). \quad (5)$$

Similar expressions may be derived for anharmonic coefficients of any order. The expressions have an

⁹ R. A. Cowley, *Advan. Phys.* **12**, 421 (1963).

¹⁰ M. Born and K. Huang, *Dynamical Theory of Crystal Lattices* (Oxford University Press, London, 1954), p. 304.

analogous form to Eq. (2) for the frequencies, which can be considered as the equation for the coefficient quadratic in the phonon coordinates.

As yet we have neglected the thermal expansion of the crystal. This arises from terms in the potential energy Eq. (3), of the form⁹

$$\sum_{\alpha} \sum_{\tau j j'} V_{\alpha\alpha}(\mathbf{q}j, -\mathbf{q}j') u_{\alpha\alpha} A(\mathbf{q}j) A(-\mathbf{q}j'),$$

where $u_{\alpha\alpha}$ is the thermal strain in the α direction. In a similar way to that described above, these coefficients can be written in terms of the potential $\phi(Q)$ as

$$\sum_{\alpha} V_{\alpha\alpha}(\mathbf{q}j, -\mathbf{q}j') = -\frac{\hbar}{Mv} \left(\frac{1}{\omega(\mathbf{q}j)\omega(\mathbf{q}j')} \right)^{1/2} \\ \times \sum_{\beta\gamma} \{K(\mathbf{q}) - K(0)\}_{\beta\gamma} u_{\beta}(\mathbf{q}j) u_{\gamma}(-\mathbf{q}j'), \quad (6)$$

where

$$\{K(\mathbf{q})\}_{\beta\gamma} = \sum_{\tau} (\mathbf{q} + \boldsymbol{\tau})_{\beta} (\mathbf{q} + \boldsymbol{\tau})_{\gamma} \\ \times [5\phi(|\mathbf{q} + \boldsymbol{\tau}|) + (\mathbf{q} + \boldsymbol{\tau}) \cdot \nabla \phi(|\mathbf{q} + \boldsymbol{\tau}|)].$$

It is of interest to note that whereas Eqs. (4) and (5) depend only on $\phi(Q)$, Eq. (6) depends on the derivative with respect to (Q) . If this derivative term is neglected in Eq. (6), the results are equivalent to the familiar Gruneisen approximation.¹⁰ In practice, however, the two terms are very similar in magnitude and we have considered both in the calculations.

4. THERMAL EXPANSION

The thermal strain may be calculated from the condition that the free energy is a minimum. The free energy is expanded about the position of static equilibrium as a power series in the strain parameters $u_{\alpha\beta}$

$$F - F_0 = \sum_{\alpha\beta} F_{\alpha\beta} u_{\alpha\beta} + \frac{1}{2} \sum_{\alpha\beta\gamma\delta} F_{(\alpha\beta)(\gamma\delta)} u_{\alpha\beta} u_{\gamma\delta}. \quad (7)$$

For an isotropic expansion, $u_{\alpha\beta} = \eta \delta_{\alpha\beta}$, the condition that the free energy is a minimum leads to

$$\sum_{\alpha} F_{\alpha\alpha} + \eta \sum_{\alpha\beta} F_{(\alpha\alpha)(\beta\beta)} = 0. \quad (8)$$

The free-energy coefficients are sums of various anharmonic terms, and to lowest order⁹

$$F_{\alpha\beta} = \sum_{\mathbf{q}j} V_{\alpha\beta}(\mathbf{q}j, -\mathbf{q}j) [2n(\mathbf{q}j) + 1],$$

and $n(\mathbf{q}j)$ is the phonon occupation number of the normal mode $(\mathbf{q}j)$. The second-order coefficients are given by the elastic constants as

$$F_{(\alpha\alpha)(\beta\beta)} = NvC_{\alpha\alpha\beta\beta}.$$

Summing Eq. (8) over α and β gives the strain in terms

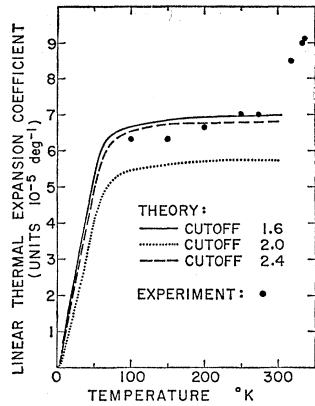


FIG. 3. Linear thermal expansion coefficient of K. The experimental results are those of Montfort and Swenson (Ref. 11) and R. H. Stokes (Ref. 12). The theoretical calculations employed the three potentials with different cutoff points shown in Fig. 1.

of the compressibility, K , since

$$\sum_{\alpha\beta} C_{\alpha\alpha\beta\beta} = \frac{9}{K}.$$

The final result for the thermal strain is

$$\eta = -\frac{K}{9vN} \sum_{qj} \sum_{\alpha} V_{\alpha\alpha}(\mathbf{q}j, -\mathbf{q}j) [2n(\mathbf{q}j) + 1]. \quad (9)$$

The thermal expansion was calculated from Eqs. (6) and (9) as a function of temperature and is shown in Fig. 3, together with the experimental measurements of Montfort and Swenson¹¹ and of Stokes.¹² In all of the calculations, the frequencies, eigenvectors, compressibility, and lattice constant were held constant at the values appropriate to 9°K. Some improvement in the agreement with experiment might be expected if they were allowed to vary with temperature, but in view of the uncertainties in the potential, this was not thought to be worthwhile. The calculations and experiment agree to well within the accuracy of the calculations, 20% as judged by the results obtained with different cutoffs. The agreement between the results with potentials having cutoffs at 1.6 and 2.4 is not surprising because the potentials themselves are very similar, as

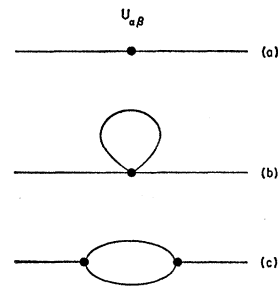


FIG. 4. The diagrams contributing to the phonon self-energy. The shift due to a strain $u_{\alpha\beta}$ is represented in part (a), that due to the mean-square displacement in part (b), and part (c) represents phonon-phonon scattering and contributes to both the shift and the lifetime.

¹¹ C. E. Montfort and C. A. Swenson, J. Phys. Chem. Solids 26, 291 (1965).

¹² R. H. Stokes, J. Phys. Chem. Solids 27, 51 (1966).

shown in Fig. 2. The remainder of the calculations in this paper were therefore performed with the cutoff of 1.6 for which the agreement with experiment is quite satisfactory. The slow rise in the experimental thermal expansion above 250°K is not reproduced by the calculations. This rise shows that higher-order anharmonic effects occur above this temperature, while the sharp rise in the measurements at 290°K probably indicates vacancy formation. Similarly, these processes have not been included in our calculations of other properties and so the calculations are expected to be in error at the highest temperatures.

5. PHONON SELF-ENERGY

A. Calculations

It has already been shown⁹ that for a weakly anharmonic crystal the self-energy of a phonon divides into a Hermitian and an anti-Hermitian part, as follows:

$$\Sigma(\mathbf{q}j, \Omega) = \Delta(\mathbf{q}j, \Omega) - i\Gamma(\mathbf{q}j, \Omega).$$

In the simple case, where there is no mixing of modes, the self-energy is diagonal in j and, provided they are small, Δ and Γ may be interpreted as the shift and width of the phonon, both of which depend on temperature and applied frequency Ω . The neutron scattering cross section is given in terms of these functions as proportional to⁹

$$\frac{1}{2\pi} \frac{1}{e^{\beta\hbar\Omega} - 1} \times \frac{4\omega(\mathbf{q}j)\Gamma(\mathbf{q}j, \Omega)}{[\omega(\mathbf{q}j)^2 + 2\omega(\mathbf{q}j)\Delta(\mathbf{q}j, \Omega) - \Omega^2]^2 + 4\omega(\mathbf{q}j)^2\Gamma(\mathbf{q}j, \Omega)^2}. \quad (10)$$

If Γ and Δ are assumed small we may assume their Ω dependence is unimportant, in which case the peak of the neutron response is given by

$$\Omega = \pm[\omega(\mathbf{q}j) + \Delta(\mathbf{q}j, \omega(\mathbf{q}j))], \quad (11)$$

and the full width at half-height of the peaks, W , is given by

$$W = 2\Gamma(\mathbf{q}j, \omega(\mathbf{q}j)). \quad (12)$$

The real and imaginary parts of the self-energies were calculated including the lowest terms in perturbation theory, which involved up to the fourth-order anharmonic coefficients. The self-energy is then the sum of the three contributions⁹ shown diagrammatically in Fig. 4, with the following result:

$$\Delta(\mathbf{q}j, \Omega) = -\frac{2}{\hbar} \sum_{\alpha} V_{\alpha\alpha}(\mathbf{q}j, -\mathbf{q}j)\eta + \frac{12}{\hbar} \sum_1 V(\mathbf{q}j, -\mathbf{q}j, \mathbf{q}_1j_1, -\mathbf{q}_1j_1)(2n_1 + 1) - \frac{18}{\hbar^2} \sum_{1,2} |V(\mathbf{q}j, -\mathbf{q}_1j_1, -\mathbf{q}_2j_2)|^2 R(\Omega)$$

and

$$\Gamma(\mathbf{q}jj\Omega) = \frac{18\pi}{\hbar^2} \sum_{1,2} |V(\mathbf{q}j, -\mathbf{q}_1j_1, -\mathbf{q}_2j_2)|^2 S(\Omega),$$

where the functions $R(\Omega)$ and $S(\Omega)$ are given by

$$R(\Omega) - i\pi S(\Omega) = \lim_{\epsilon \rightarrow 0} \{ (n_1 + n_2 + 1) \\ \times [(\Omega + \omega_1 + \omega_2 + i\epsilon)^{-1} - (\Omega - \omega_1 - \omega_2 + i\epsilon)^{-1}] + (n_2 - n_1) \\ \times [(\Omega - \omega_1 + \omega_2 + i\epsilon)^{-1} - (\Omega + \omega_1 - \omega_2 + i\epsilon)^{-1}] \}, \quad (13)$$

and where the labels 1, 2 represent (\mathbf{q}_1j_1) , (\mathbf{q}_2j_2) , respectively. The off-diagonal elements of the self-energy are identically zero in the present case because each mode belongs to one irreducible representation for the symmetric directions we have considered.

The summations over \mathbf{q} were performed on a finite mesh of different points within the Brillouin zone. The size of ϵ was chosen to be 0.1×10^{12} Hz in the final calculations, which seemed to give sufficient sampling of the frequencies by the points of the mesh. Independent calculations, performed on meshes with 1000 and 2000 points within the Brillouin zone, gave essentially the same results.

In calculations of the phonon self-energies, as in those of the thermal strain, no account was taken of renormalization of the frequencies appearing in the above formulas. The frequencies, lattice constant, and elastic constants were those appropriate to 9°K. These quantities are practically the same as those of the position of static equilibrium as shown in Table III, where the thermal strain and the anharmonic self-energy of a typical phonon is shown to be negligible at 9°K.

The real and imaginary parts of the self-energies were calculated for several values of frequencies Ω around the anharmonic frequencies $\omega(\mathbf{q}j)$. In Fig. 5, we show the resulting shape of two of the most heavily attenuated modes. The results have close to a Lorentzian shape and so it is a reasonable approximation to consider the frequency as given by Eq. (11) and the width by Eq. (12). Likewise, no evidence was found experimentally for any neutron group having a shape inconsistent with this approximation.

The calculated widths and shifts at 9, 92, 215, and 299°K are shown in Table IV. The contributions to the shift in frequency (Δ) from thermal expansion (Δ_T), the fourth-order coefficient (Δ_4), and the third-order coefficient (Δ_3) are individually given. For most modes, the largest contribution to the shift is from the thermal strain. For some modes the third- and fourth-order contributions are of opposite sign and partially cancel, as was found in alkali halides.¹³ There are many branches, however, where all three contributions are of the same sign, for example, H_{15} , Σ_3 , and N_3' . For other branches, Δ_4 is positive but sufficiently small so that no

¹³ E. R. Cowley and R. A. Cowley, Proc. Roy. Soc. (London) **A287**, 259 (1965).

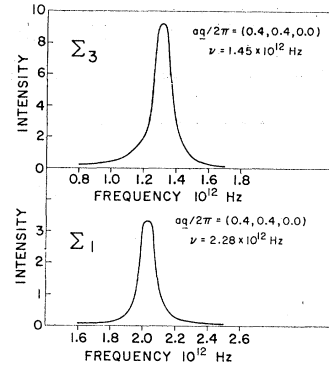


FIG. 5. Computed shapes of two neutron groups in K at room temperature.

appreciable cancellation takes place, for example, Λ_1 , F_1 , F_3 , Σ_1 , and N_1' . For all these branches the numerical accuracy of the calculations is probably of the same order (20%) as the calculation of thermal expansion. For a few modes where the contributions to the shift largely cancel, for example, G_1 , N_4' , Λ_3 , the accuracy will be less and may be estimated by assigning a 20% error to the individual contributions.

The small oscillations observed, for example, in the calculations for modes Δ_5 , are probably not significant and are the result of using a cutoff potential. On the other hand, the large oscillation for the shift of the $\Lambda_1(F_1)$ modes is significant. Its shape is clearly related to that of the harmonic frequency in this direction,¹ and the experimental results are also consistent with an oscillation in the shift for $\Lambda_1(F_1)$ modes.

6. COMPARISON OF THEORY AND EXPERIMENT

In Fig. 6, the measured changes in the frequency and the half-widths of the neutron groups are compared with the theoretical calculations described in Sec. 5. The agreement between the calculations and experiment is quite satisfactory for the frequency changes but less so for the widths. In particular, the results for the changes in the Σ_1 , Σ_3 and Λ_3 branches given are in excellent agreement. Those for the Λ_1 and Δ_5 branches agree at 90 and 215°K but the calculations are somewhat too small at 299°K. This may indicate that the scattering by vacancies has an appreciable effect on these frequencies at high temperatures.

It is clear from the scatter in the measurements of the width that a comparison of individual results with

TABLE III. Anharmonic effects at 9°K.

Thermal strain η Mode $\mathbf{q} = 2\pi/a(0,0,1,0)$	0.22%
Frequency $\omega(\mathbf{q}j)$	2.21×10^{12} Hz
Shift $\Delta(\mathbf{q}jj, \omega(\mathbf{q}j))$	-0.036×10^{12} Hz
Half-width $\Gamma(\mathbf{q}jj, \omega(\mathbf{q}j))$	0.005×10^{12} Hz

TABLE IV. Calculated widths and shifts in potassium in units 10^{12} Hz. The four rows of data following each mode refer successively to temperatures 299, 215, 92, and 9°K. The individual contributions to the shift from the strain and from the third- and fourth-order coefficients are also tabulated. The change in the shift and width from their 9°K values is shown in the last two columns.

Wave vector	Mode	Frequency	Δ_T	Δ_1	Δ_3	Δ	Γ	$\delta\Delta$	$\delta\Gamma$
(0,0,0,0,2)	Δ_5	0.69	-0.029	-0.044	-0.037	-0.110	0.020	-0.100	0.020
			-0.021	-0.032	-0.027	-0.080	0.015	-0.070	0.015
			-0.009	-0.014	-0.012	-0.035	0.006	-0.025	0.006
			-0.004	-0.003	-0.003	-0.010	0.000		
(0,0,0,0,4)	Δ_5	1.29	-0.049	-0.062	-0.046	-0.157	0.046	-0.139	0.045
			-0.036	-0.045	-0.033	-0.114	0.033	-0.096	0.032
			-0.016	-0.020	-0.016	-0.052	0.014	-0.034	0.013
			-0.000	-0.005	-0.007	0.018	0.001		
(0,0,0,0,6)	Δ_5	1.79	-0.080	-0.071	-0.074	-0.225	0.041	-0.199	0.039
			-0.058	-0.051	-0.049	-0.158	0.030	-0.132	0.028
			-0.026	-0.022	-0.023	-0.071	0.013	-0.045	0.011
			-0.010	-0.005	-0.011	-0.026	0.002		
(0,0,0,0,8)	Δ_5	2.11	-0.099	-0.068	-0.119	-0.256	0.061	-0.223	0.056
			-0.072	-0.049	-0.086	-0.207	0.044	-0.174	0.039
			-0.033	-0.021	-0.039	-0.093	0.019	-0.060	0.014
			-0.013	-0.005	-0.015	-0.033	0.005		
(0,0,0,0,1,0)	H_{15}	2.21	-0.112	-0.062	-0.155	-0.329	0.061	-0.293	0.056
			-0.081	-0.045	-0.112	-0.238	0.044	-0.202	0.039
			-0.037	-0.019	-0.050	-0.106	0.019	-0.070	0.014
			-0.014	-0.004	-0.018	-0.036	0.005		
(0,2,0,2,0,0)	Σ_1	1.43	-0.088	0.003	-0.044	-0.129	0.025	-0.113	0.024
			-0.064	0.002	-0.032	-0.094	0.018	-0.078	0.017
	Σ_3	0.93	-0.029	0.001	-0.014	-0.042	0.008	-0.026	0.001
			-0.011	0.002	-0.007	-0.016	0.001		
(0,3,0,3,0,0)	Σ_1	1.98	-0.035	-0.064	-0.044	-0.143	0.028	-0.130	0.028
			-0.026	-0.046	-0.032	-0.104	0.020	-0.091	0.020
	Σ_3	1.24	-0.012	-0.020	-0.014	-0.046	0.008	-0.035	0.008
			-0.004	-0.005	-0.004	-0.013	0.000		
(0,4,0,4,0,0)	Σ_1	2.28	-0.133	0.021	-0.066	-0.178	0.034	-0.155	0.031
			-0.096	0.015	-0.048	-0.129	0.025	-0.106	0.022
	Σ_3	1.45	-0.044	0.007	-0.022	-0.059	0.011	-0.036	0.008
			-0.017	0.004	-0.010	-0.023	0.003		
(0,5,0,5,0,0)	N_1'	2.40	-0.043	-0.076	-0.054	-0.173	0.041	-0.156	0.040
			-0.031	-0.055	-0.039	-0.125	0.029	-0.108	0.028
	N_3'	1.52	-0.014	-0.024	-0.018	-0.056	0.012	-0.039	0.011
			-0.005	-0.006	-0.006	-0.017	0.001		
(0,4,0,4,0,0)	Σ_1	2.28	-0.171	0.041	-0.097	-0.227	0.062	-0.198	0.057
			-0.124	0.030	-0.070	-0.164	0.045	-0.135	0.040
	Σ_3	1.45	-0.056	0.014	-0.032	-0.074	0.020	-0.045	0.015
			-0.022	0.006	-0.013	-0.029	0.005		
(0,5,0,5,0,0)	N_1'	2.40	-0.057	-0.085	-0.056	-0.198	0.050	-0.178	0.049
			-0.041	-0.061	-0.041	-0.143	0.036	-0.123	0.035
	N_3'	1.52	-0.019	-0.027	-0.018	-0.064	0.015	-0.044	0.014
			-0.007	-0.006	-0.007	-0.020	0.001		
(0,4,0,6,0,0)	N_4'	0.53	-0.176	0.045	-0.098	-0.229	0.066	-0.200	0.060
			-0.128	0.032	-0.071	-0.167	0.047	-0.138	0.041
	N_3'	1.52	-0.058	0.015	-0.032	-0.075	0.021	-0.046	0.015
			-0.022	0.006	-0.013	-0.029	0.006		
(0,4,0,6,0,0)	N_4'	0.53	-0.055	-0.089	-0.053	-0.197	0.048	-0.176	0.047
			-0.040	-0.064	-0.039	-0.143	0.034	-0.122	0.033
	N_3'	1.52	-0.018	-0.028	-0.018	-0.064	0.015	-0.043	0.014
			-0.007	-0.007	-0.007	-0.021	0.001		
(0,4,0,6,0,0)	G_1	0.79	-0.062	0.301	-0.127	+0.112	0.081	+0.112	0.080
			-0.045	0.216	-0.092	+0.079	0.057	+0.079	0.056
	F_1	1.45	-0.020	0.093	-0.040	+0.033	0.022	0.033	0.021
			-0.008	0.016	-0.008	0.000	0.001		
(0,4,0,6,0,0)	G_1	0.79	-0.056	0.189	-0.120	+0.013	0.056	+0.019	0.055
			-0.040	0.136	-0.086	+0.010	0.041	0.016	0.040
	F_1	1.45	-0.018	0.058	-0.037	+0.003	0.016	0.009	0.015
			-0.007	0.010	-0.009	-0.006	0.001		
(0,2,0,2,0,8)	F_1	1.45	-0.066	-0.005	-0.100	-0.171	0.062	-0.150	0.061
			-0.048	-0.004	-0.072	-0.124	0.045	-0.103	0.044
	F_3	2.15	-0.022	-0.002	-0.032	-0.056	0.019	-0.035	0.018
			-0.008	-0.002	-0.011	-0.021	0.001		
(0,4,0,4,0,6)	F_1	1.28	-0.128	-0.019	-0.111	-0.258	0.076	-0.217	0.070
			-0.093	-0.014	-0.080	-0.187	0.055	-0.156	0.049
	F_1	1.28	-0.042	-0.006	-0.036	-0.084	0.024	-0.053	0.018
			-0.016	-0.000	-0.015	-0.031	0.006		
(0,4,0,4,0,6)	F_1	1.28	-0.090	0.078	-0.130	-0.142	0.090	-0.124	0.086
			-0.065	0.056	-0.093	-0.102	0.065	-0.084	0.061
	F_1	1.28	-0.029	0.024	-0.041	-0.046	0.028	-0.028	0.024
			-0.011	0.005	-0.012	-0.018	0.004		

TABLE IV. (continued).

Wave vector	Mode	Frequency	Δ_T	Δ_4	Δ_3	Δ	Γ	$\delta\Delta$	$\delta\Gamma$	
(0.4,0.4,0.6)	F_3	1.99	-0.142	0.041	-0.079	-0.180	0.051	-0.155	0.047	
			-0.103	0.029	-0.057	-0.131	0.037	-0.006	0.033	
			-0.047	0.013	-0.026	-0.060	0.016	-0.035	0.012	
(0.4,0.4,0.4)	Λ_1	2.14	-0.018	0.005	-0.012	-0.025	0.004			
			-0.154	0.032	-0.095	-0.217	0.061	-0.190	0.056	
			-0.112	0.023	-0.069	-0.158	0.044	-0.131	0.039	
	Λ_3	1.54	-0.051	0.011	-0.030	-0.070	0.019	-0.043	0.014	
			-0.019	0.005	-0.013	-0.027	0.005			
			-0.110	0.061	-0.087	-0.136	0.059	-0.115	0.056	
(0.2,0.2,0.2)	Λ_1	1.71	-0.080	0.044	-0.063	-0.099	0.042	-0.078	0.039	
			-0.036	0.019	-0.029	-0.046	0.018	-0.025	0.015	
			-0.014	0.004	-0.011	-0.021	0.003			
	Λ_3	0.79	-0.103	-0.010	-0.046	-0.159	0.041	-0.139	0.039	
			-0.075	-0.007	-0.034	-0.116	0.030	-0.096	0.028	
			-0.034	-0.003	-0.015	-0.052	0.013	-0.032	0.011	
	(0.1,0.1,0.9)	F_1	1.99	-0.013	+0.001	-0.008	-0.020	0.002		
				-0.038	0.041					
				-0.028	0.030					
F_3		2.19	-0.013	0.013						
			-0.005	0.002						
(0.3,0.3,0.7)	F_1	1.01								
	F_3	2.10								
(0.5,0.5,0.5)	F_1, F_3	1.80								
(0.3,0.3,0.3)	Λ_1	2.11								
	Λ_3	2.11								

the theory is not meaningful (see Table II for the errors). However, Fig. 6 shows that the over-all trend of both theory and experiment are similar, although the calculated half-widths are about half the measured ones for most branches. This discrepancy in the widths may indicate that there are processes which scatter the phonons which we have not taken into account. These might include the effects of vacancies and higher-order anharmonicities, which, as can be seen from the thermal expansion (Fig. 3), are important at the highest temperatures. Further possibilities are discussed in Sec. 7, in which the validity of the neutral-pseudoatom approach is considered. However, we cannot rule out the possibility that a large part of the discrepancy arises because we have not extracted the experimental resolution function adequately. If the one-phonon cross sections are not Lorentzian in shape or if the resolution function is not Gaussian, then considerable changes occur in our

results. Furthermore, the change in the frequencies with temperature alters the resolution function and we have neglected these changes in our analysis.

The agreement between theory and experiment is therefore satisfactory for the frequency shifts but is less so for the widths. Before drawing any conclusions as to whether the disagreement for the widths is significant, we shall examine the pseudopotential theory in greater detail with particular attention to contributions to the phonon lifetimes.

7. PSEUDOPOTENTIAL ANALYSIS

A. Ion-Electron-Ion Interaction

In the foregoing sections we have used the neutral-pseudoatom model to discuss anharmonic effects in potassium. In this section we discuss the validity of this approximation. The forces between the ions in a metal

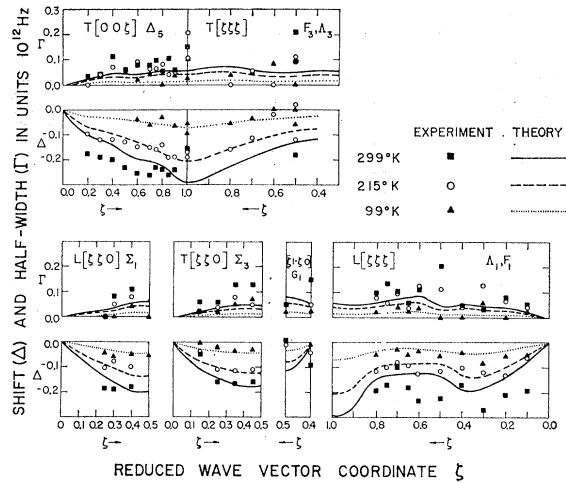


FIG. 6. Shifts and half-widths in K at three temperatures. The points are neutron scattering measurements and the lines are theoretical calculations made with the potential between neutral pseudoatoms derived from 90°K data. Squares and solid lines are for 299°K, circles and dashed lines for 215°K, and triangles and dotted lines for 92°K.

arise partly from the direct ion-ion interaction. In the alkali metals this is well approximated by the electrostatic interactions $\phi_e(\mathbf{Q})$ between the ion charges. In addition, there is the interaction through the conduction electrons. This interaction is shown diagrammatically in Fig. 7, and the total ion-ion potential is given by²⁻⁷

$$\phi(\mathbf{Q}) = \phi_e(\mathbf{Q}) - \pi(\mathbf{Q}) |V(\mathbf{Q})|^2 / \epsilon(\mathbf{Q}), \quad (14)$$

where $V(\mathbf{Q})$ is the electron-ion pseudo-potential, $\epsilon(\mathbf{Q})$ the electron dielectric constant which in the Hartree self-consistent field approximation is

$$\epsilon(\mathbf{Q}) = 1 + (4\pi e^2 / Q^2) \pi(\mathbf{Q}), \quad (15)$$

and $\pi(\mathbf{Q})$ is the electron polarization operator,

$$\pi(\mathbf{Q}) = \frac{1}{N} \sum_{\mathbf{k}} \frac{n(\mathbf{k}) - n(\mathbf{k} + \mathbf{Q})}{E(\mathbf{k}) - E(\mathbf{k} + \mathbf{Q})}. \quad (16)$$

The electron of state \mathbf{k} has occupation number $n(\mathbf{k})$ and energy $E(\mathbf{k})$.

One difference between this potential¹⁴ and the neutral-pseudoatom potential assumed in Sec. 3 is

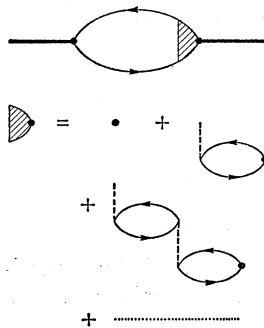


FIG. 7. Phonon self-energy caused by the ion-electron-ion interaction. The heavy lines are phonons, the light lines electrons, and the dotted lines the photons involved in the screening of the electron-ion interaction. The same convention is followed in subsequent figures.

¹⁴ J. J. Kokkedee, *Physica* **28**, 983 (1962).

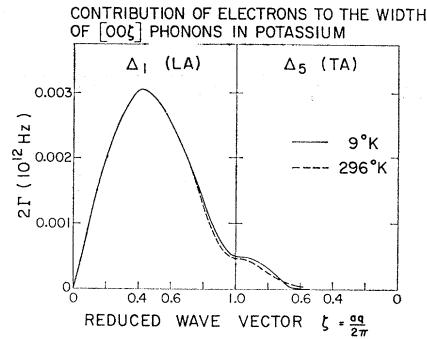


FIG. 8. The phonon width in the [100] direction in K arising from the imaginary part of the dielectric polarization.

that the ion-electron-ion interaction gives some scattering of the phonons.^{14,15} This depends on the imaginary part of $\pi(\mathbf{Q})$ of Eq. (14). However, since few electrons lie within a typical phonon energy of the Fermi surface, the resulting width of the phonon groups is comparatively small. Figure 8 shows the width calculated for the [100] direction in potassium. Also shown in Fig. 8 is the temperature dependence of this width which, because the Fermi temperature is large compared with the temperatures of the experiment, is quite negligible. Consequently, since we have only measured the increase in the width of the neutron groups with temperature, the scattering of the phonons by the electrons does not significantly alter our results.

B. Anharmonic Interactions

In Fig. 9, we show the two different types of diagram which make up the ion-electron-ion contribution to the cubic anharmonic interactions of Eq. (3). Diagram (a) has two pseudopotential interactions and corresponds to a two-body interaction. Its contribution is very similar to that of the electronic part of Eq. (14), and together with the Coulomb interaction it is treated exactly by the pseudoatom approximation of Sec. 3.

Diagram (b) of Fig. 9 is considerably more complex and to our knowledge has not been discussed in the literature. It contains three pseudopotential interactions and consequently corresponds to a three-body potential. Although its contribution can be evaluated by the use of

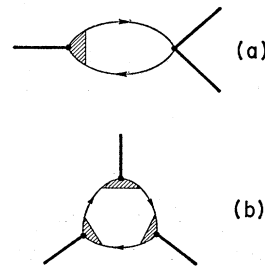
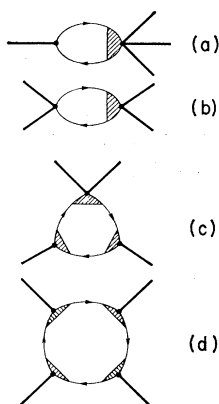


FIG. 9. Cubic anharmonic interaction between phonons via the electrons. Diagram (a) is a two-body interaction and (b) is a three-body interaction.

¹⁵ J. Bjorkman, B. I. Lundqvist, and A. Sjolander, *Phys. Rev.* **159**, 551 (1967).

FIG. 10. Quartic anharmonic interaction between phonons. Diagrams (a) and (b) are two-body interactions, while (c) and (d) are three- and four-body interactions.

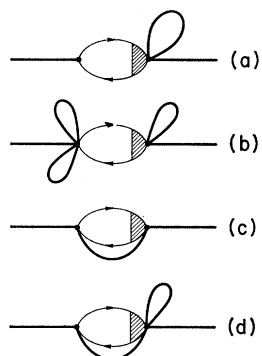


the familiar rules for diagrams,¹⁶ at least formally, we have been unable to perform the resulting integrals over the electron momentum analytically. This makes calculations of this term extremely lengthy and so we have not attempted any numerical computation of its magnitude. Since the term involves three pseudopotentials, whereas diagram (a) contributes only two, it is tempting to suggest it will therefore be smaller, but we have been unable to justify this argument. The only suggestion we can put forward is that it seems likely that three-body forces will be less important than two-body ones. Furthermore, this term also contributes to the thermal expansion and our pseudoatom approximation, for it gave quite satisfactory agreement with experiment.

In Fig. 10 we show the different contributions to the quartic anharmonicity. As with the cubic terms, the two-body terms, diagrams (a) and (b), are treated exactly by the pseudoatom approximation but the three-body interactions, diagram (c), and the four-body ones, diagram (d), are neglected. As with the cubic anharmonicity, we have no real justification for this other than the practical difficulty of including them.

There are other diagrams which contribute to the phonon self-energy. Some of these involve the simultaneous excitation of both electrons and phonons. Their contributions are, however, smaller than those of the

FIG. 11. Diagrams contributing to the Kohn anomaly in metals.



¹⁶ A. A. Abrikosov, L. P. Gorkov, and J. E. Dzyaloshinski, *Methods of Quantum Field Theory in Statistical Physics* (Prentice-Hall, Inc., Englewood Cliffs, N. J., 1963).

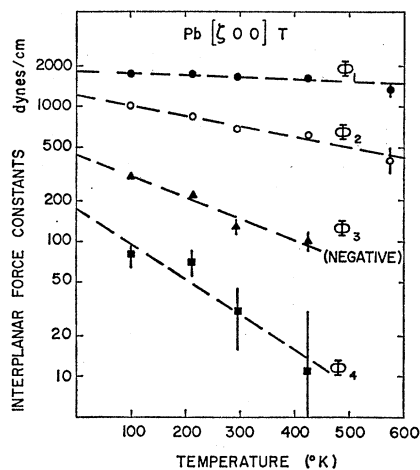


FIG. 12. Interplanar force constants in lead as a function of temperature (Ref. 18).

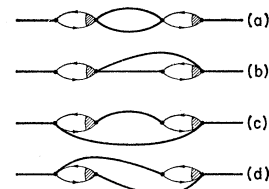
diagrams we have discussed because they may be shown to belong to higher terms in the phonon expansion.

C. Kohn Anomalies

Although the Kohn anomalies¹⁷ in potassium are too small to be detected experimentally, it is of some interest to discuss, in general, the way in which anharmonic effects modify Kohn anomalies with temperature. Since the expressions for the anharmonic coefficients [Eqs. (4) and (5)] involving a particular wave vector \mathbf{q} include contributions from $\phi(|\mathbf{q}+\boldsymbol{\tau}|)$, these anharmonic coefficients will also exhibit Kohn anomalies. The widths and changes of frequency considered as functions of \mathbf{q} will therefore exhibit Kohn anomalies whenever $|\mathbf{q}+\boldsymbol{\tau}|=2k_F$, and these will modify the size of the anomalies.

This behavior is illustrated by the diagrams shown in Fig. 11. The structure of the diagrams is very similar to those describing the inelastic scattering of radiation by harmonic crystal.⁹ Diagrams (a) and (b) correspond to the Debye-Waller factor while (c) is a one-phonon diagram and (d) a two-phonon diagram. The important feature for the present purposes is the set of diagrams which contribute to the Kohn anomaly. These are the no-phonon scattering diagrams such as (a) and (b); we clearly incorporate all the multiphonon effects of these diagrams by multiplying the size of the Kohn

FIG. 13. Cubic anharmonic diagrams showing the different ways in which the electron-hole pairs enter.



¹⁷ W. Kohn, *Phys. Rev. Letters* 2, 393 (1959).

anomaly by the Debye-Waller factor. The anomalies for the one- and two-phonon diagrams, (c) and (d), occur at different wave vectors depending on the wave vectors of both the incident and scattered phonons. When averaged over all possible processes they do not give anomalies at particular wave vectors. For the class of diagrams shown in Fig. 11, therefore, we expect the Kohn anomalies to have a temperature dependence given by the well-known Debye-Waller factor. Consequently, they will decrease in size with increasing temperature. This may be the explanation of the result found in lead,¹⁸ Fig. 12, which shows the range of the interatomic forces decreasing rapidly with increasing temperature.

It is more difficult to assess the effect of more complex diagrams on the Kohn anomalies. The cubic anharmonic diagrams are shown in Fig. 13. Diagrams (a) and (b) contribute to the Kohn anomaly while diagrams (c) and (d) do not. The sign of the contribution may be either positive or negative in the same way that the cubic anharmonic shift may be positive or negative. However, since this term also contributes to the width of the group, it seems unlikely that in practice it will give rise to large anomalies because the width will tend to blur out any sharp features.

8. DISCUSSION AND CONCLUSIONS

A study has been made of anharmonicity in potassium metal. We have measured the temperature dependence of many phonons, and have found that the frequency shifts and widths and also the thermal expansion can be reasonably explained by calculations based on the neutral pseudoatom approximation, when only the lowest terms in an anharmonic expansion are included. The pseudoatom potential was obtained from the measured phonon frequencies at 9°K.

The most difficult part of the experimental work is the extraction of the experimental resolution function from the measurements. This was done by comparing

¹⁸ B. N. Brockhouse, T. Arase, G. Gaglioti, M. Sakamoto, R. N. Sinclair, and A. D. B. Woods, in *Inelastic Scattering of Slow Neutrons from Solids and Liquids* (International Atomic Energy Agency, Vienna, 1961).

the high-temperature results with the results at 9°K. However, there is still some uncertainty in the resulting width because the shape of both the one-phonon cross section and the resolution function are somewhat uncertain. Although we have verified that the observed neutron groups have the expected shapes, a large part of the error in our measured widths comes from this source. A problem that always exists is that anharmonic effects mix the one-phonon peak with the background so as to alter both the peak shape¹⁹ and its intensity.²⁰ Our results for the widths at the highest temperatures may be in error from this cause.

On the theoretical side we have developed a method for calculating anharmonic effects which uses the same potential that enters into the calculation of harmonic phonon frequencies. The electronic band structure may also be calculated from this potential if the dielectric constant is known. The method is applicable to all simple metals. We have neglected, however, the three- and four-body forces which occur explicitly in the pseudopotential formalism for the anharmonic coefficients. Their inclusion would be very difficult in practice at the present time. Nevertheless, the fact that we obtain reasonable agreement between experiment and theory for both the shifts in frequency and the thermal expansion does suggest that the many-body forces are much smaller than the two-body forces. We hope this result will stimulate further theoretical work to demonstrate this more satisfactorily.

In conclusion, therefore, we have shown that a neutral-pseudoatom potential, which gives an excellent account of the harmonic lattice dynamics of potassium, also gives a reasonable description of the anharmonic effects.

ACKNOWLEDGMENTS

We have benefitted from discussions with many colleagues at Chalk River and from the invaluable assistance of E. A. Glaser in performing the experiments.

¹⁹ V. Ambegaokar, J. Conway, and G. Baym, in *Lattice Dynamics*, edited by R. F. Wallis (Pergamon Press, Inc., New York, 1965), p. 261; A. A. Maradudin and V. Ambegaokar, *Phys. Rev.* **135**, A1070 (1964).

²⁰ R. A. Cowley and W. J. L. Buyers (unpublished).